

# Dzyaloshinskii-Moriya interaction inducing weak ferromagnetism in centrosymmetric altermagnets and weak ferrimagnetism in noncentrosymmetric altermagnets

Carmine Autieri<sup>ib</sup>,<sup>1,\*</sup> Raghottam M Sattigeri<sup>ib</sup>,<sup>1,†</sup> Giuseppe Cuono<sup>ib</sup>,<sup>1,‡</sup> and Amar Fakhredine<sup>2</sup>

<sup>1</sup>*International Research Centre Magtop, Institute of Physics,  
Polish Academy of Sciences, Aleja Lotników 32/46, 02668 Warsaw, Poland*

<sup>2</sup>*Institute of Physics, Polish Academy of Sciences, Aleja Lotników 32/46, 02668 Warsaw, Poland*

The Dzyaloshinskii-Moriya interaction (DMI) has explained successfully the weak ferromagnetism in *some* centrosymmetric antiferromagnets. However, in the last years, it was generally claimed that the DMI is not effective in centrosymmetric systems. We reconciled these views by separating the conventional antiferromagnets and altermagnets. Altermagnets represent collinear antiferromagnetic compounds with spin-up and spin-down sublattices connected only by mirror and roto-translational symmetries. Consequently, the system shows even-parity wave spin order in the k-space lifting the Kramer's degeneracy in the non-relativistic band structure. We emphasize that the DMI can create weak ferromagnetism in centrosymmetric altermagnets while it is not effective in centrosymmetric conventional antiferromagnets. Additionally, DMI can create weak ferromagnetism or weak ferrimagnetism in noncentrosymmetric altermagnets. Once the spin-orbit coupling is included in an altermagnetic system without time-reversal symmetry, the components of spin moments of the two sublattices along the Néel vector are antiparallel but the other two spin components orthogonal to the Néel vector can be either parallel or antiparallel for centrosymmetric systems. For noncentrosymmetric systems, we can have different bands showing parallel or antiparallel spin components resulting in weak ferrimagnetism. We can divide the altermagnetic compounds into classes based on the weak ferromagnetism or weak ferrimagnetism properties. In the case of weak ferromagnetism, the Hall vector is orthogonal to the Néel vector while in the case of weak ferrimagnetism the Hall vector has a component parallel to the Néel vector too. Therefore, an electric field breaking the inversion symmetry could generate a magnetization parallel to the Néel vector. We find a sign change of the magnetization, and possibly of the anomalous Hall effect, as a function of the band filling and Néel vector. We describe the dependence of the weak ferromagnetism from the charge doping and electric field. The weak ferromagnetism and weak ferrimagnetism induced by DMI is a property exclusively of the altermagnets, not present in either ferromagnets or conventional antiferromagnets so we propose that altermagnets should be classified based on this property.

## I. INTRODUCTION

It was discovered that non-relativistic spin-splitting in electronic bands can be a feature in antiferromagnetic materials having two equivalent sublattices with magnetic moments related by crystal-symmetry<sup>1,2</sup>. This magnetic phase has been named altermagnetism (AM)<sup>3-7</sup> or antiferromagnetism with non-interconvertible spin-structure motif pair<sup>8</sup>. The existence of AM necessitates that the electronic charge of spin-up (down) atoms should be mapped into spin-down (up) atoms not exclusively via translations, inversions, or their combinations but through the application of roto-translations or mirrors<sup>6,7</sup>. As a result, AM can be observed in specific space groups, and more precisely, in the magnetic space groups of type-I and type-III<sup>9</sup>. Numerous transition metal oxides<sup>9</sup> and rare-earth compounds have been documented to present altermagnetism<sup>10</sup>. Altermagnets have a wide range of potential applications, they are promising to enable highly efficient spin-current generation<sup>11</sup>, as well as contributing to the development of giant and tunneling magnetoresistance<sup>12</sup>. It was shown that spin-independent conductance in altermagnets can be efficiently exploited in spintronics<sup>13-15</sup>. Furthermore, altermagnets can play a significant role in spin caloritronics<sup>16</sup> and can be practical use in Josephson junctions<sup>17</sup>.

The Dzyaloshinskii-Moriya interaction (DMI) is a relativistic magnetic interaction that has successfully explained the weak ferromagnetism described for the first time in centrosymmetric antiferromagnets<sup>18-20</sup> with space group 167. This weak ferromagnetism has a relativistic origin and is the only kind of weak ferromagnetism discussed in this paper. Some compounds of the centrosymmetric space group 62 exhibit weak ferromagnetism and lead to a significant ferromagnetic behavior, which was later explained by the mechanism of the Dzyaloshinskii-Moriya exchange based on torque measurements<sup>21,22</sup>. The spin canting has been attributed to the DMI in most cases, although other effects share the same requirements to be imposed on the crystal symmetry<sup>23</sup>. The weak ferromagnetism can also be present in complex systems like solids with molecules as cations<sup>24</sup> and biphasic systems<sup>25</sup>. In other literature, the weak ferromagnetism from DMI in bulk systems was associated with noncentrosymmetric systems<sup>26</sup>. Furthermore, in ferroelectric BiFeO<sub>3</sub>, a subtle DMI which constitutes about 1% of the antiferromagnetic exchange strength causes a tilting of the two spin sublattices, consequently giving rise to "weak ferromagnetism"<sup>20,27</sup>. The DMI as explained by definition, appears as an effect of antisymmetric interactions, which necessitates a lack of inversion symmetry between two spins. Nevertheless, a structure can possess an overall centrosymmet-

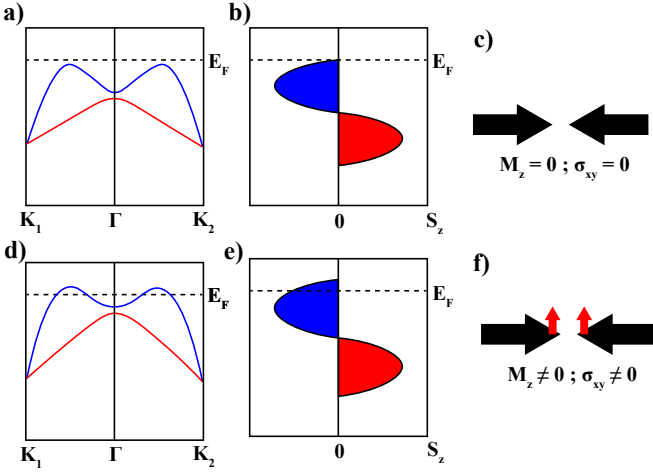


FIG. 1. Origin of weak ferromagnetism in altermagnets. (a) Schematic band structure of an altermagnet with SOC, Néel vector in the  $xy$  plane and Fermi level in the gap. The red and blue colors represent the negative and positive  $S_z$  component of the total system. (b) Local  $S_z$  component for the magnetic atom as a function of the energy for the energy spectrum (a), in the centrosymmetric case  $S_z$  for the two atoms are equal. (c) Magnetic configuration without  $M_z$  and AHE  $\rho_{xy}$ . (d) Same as (a) with metallicity. (e)  $S_z$  component as a function of the energy for the energy spectrum (d). (f) Magnetic configuration with non-zero  $M_z$  components and non-zero AHE  $\rho_{xy}$ .

ric crystal symmetry while also accommodating a DMI interaction<sup>28</sup>. DMI plays an important role in forming skyrmions with a fixed chirality and vorticity in the case of noncentrosymmetric magnets since it allows the tilting of adjacent spins under special rules related to crystal symmetry. In contrast, in centrosymmetric structures, other mechanisms are believed to be responsible for complex magnetism<sup>29</sup>.

The non-relativistic spin-splitting is proportional to the hopping parameters which tend to increase with the atomic number. Large spin-splittings have been found in compounds with heavy elements as MnTe, RuO<sub>2</sub>, CrSb, etc ... which are also the most representative and most studied compounds among the altermagnetic systems. Beyond the large spin-splitting, these heavy atoms own a huge spin-orbit coupling (SOC). Therefore, the study of the spin-orbital effects is extremely relevant, especially for the most representative altermagnets. Beyond that, the anomalous Hall effect (AHE) strongly depends on the size of the SOC. In the case of a metallic system, the DMI produces weak ferromagnetism in AM compounds that display spontaneous AHE<sup>3,30</sup> which can be enhanced by Weyl points<sup>31</sup>. The orientation of the Hall vector strongly depends on the Néel vector, which is defined as the difference between the magnetization vectors of the two distinct magnetic sublattices<sup>15,32,33</sup>. While the direction of the Hall vector has been explored using symmetry considerations, there is a notable absence of information in the literature regarding how to establish this orienta-

tion based on fundamental electronic properties through density functional theory calculations.

In this work, our objective is to have a general understanding of the appearance of weak ferromagnetism in centrosymmetric systems, while we found weak ferromagnetism and weak ferrimagnetism in noncentrosymmetric systems. We discuss why weak ferromagnetism and weak ferrimagnetism are relativistic effects that can appear only in altermagnets. Once the time-reversal symmetry is broken and the Kramers degeneracy is lifted, the spin components of the two sublattices orthogonal to the Néel vector are related by symmetry in centrosymmetric systems and therefore must be parallel or antiparallel. The scenario changes in noncentrosymmetric systems where different sets of bands can generate at the same time parallel or antiparallel spin components in which we establish that the direction of the Hall vector is orthogonal to the Néel vector. A schematic representation of our main results is presented in Fig. 1. We propose that the band structure reported in Fig. 1(a) can be present in all altermagnets for a suitable Néel vector, as a consequence of this band structure, the local density of states (DOS) for the component of the spin orthogonal to the Néel vector have a relativistic spin-splitting as shown in 1(b). If the Fermi level is in the gap, we still observe a net zero magnetic configuration  $M_z$  and zero anomalous Hall effect in altermagnets owing to a complete antiparallel spin configuration in two sublattices. However, when bands cross the Fermi level (as in Fig. 1(d)) which is also evident from the increase in the contribution from the  $S_z$  component (as in Fig. 1(e)), the SOC creates an effective non-zero magnetic configuration giving rise to ferromagnetic spins aligned perpendicular to the Néel vector (as in Fig. 1(f)) leading to a non-zero anomalous Hall effect in altermagnetic compounds. Integrating in energy the spin component orthogonal to the Néel in a realistic multiband system we will obtain the magnetization as a function of the energy, this magnetization can be zero at the same energies by compensation of the spins, however, the compensation of the spins does not mean that we have a compensation of the Berry curvature. Therefore, a null magnetization is not associated with a null anomalous Hall effect<sup>34</sup>. The weak ferromagnetism is difficult to detect especially on the nanoscale level, so our work provides a guide to theoretically predict the direction of the weak ferromagnetism to support the experimental investigation. Using density functional theory calculations, the results of the self-consistent calculation will report parallel or antiparallel components depending on which of them minimizes the total energy. We calculate the spin components of the two sublattices as a function of the Néel vector for the centrosymmetric d-wave RuO<sub>2</sub>, the centrosymmetric g-wave CrSb and the noncentrosymmetric g-wave MnSe. The paper is organized as follows: the second Section describes the computational framework while the third Section is dedicated to the results for the three chosen compounds. Finally, in the fourth Section, the authors draw their conclusions.

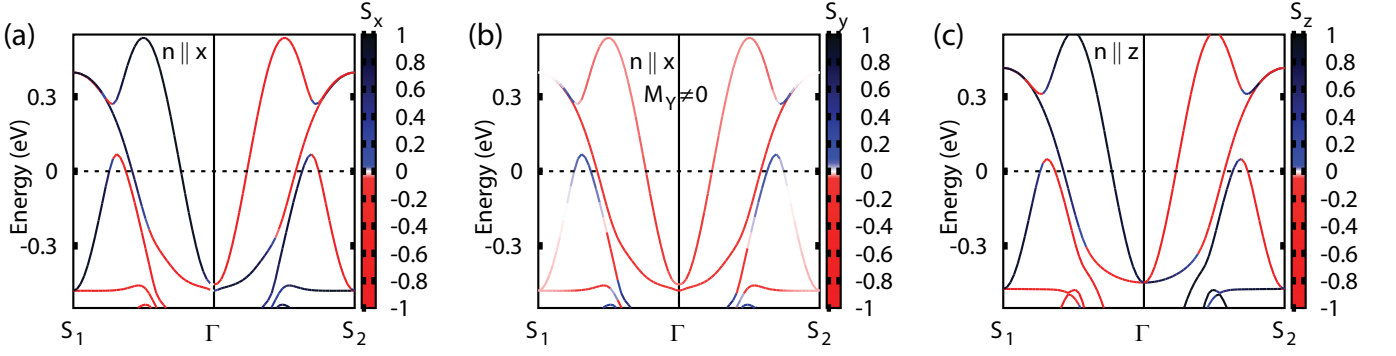


FIG. 2. Band structure of d-wave RuO<sub>2</sub> along the S<sub>1</sub>-Γ-S<sub>2</sub> low-symmetry k-path. (a) The positive and negative S<sub>x</sub> components are plotted in red and blue, respectively, while the Néel vector is along the x-axis. (b) The positive and negative S<sub>y</sub> components are plotted in red and blue, respectively, while the Néel vector is along the x-axis. (c) The positive and negative S<sub>z</sub> components are plotted in red and blue, respectively, while the Néel vector is along the z-axis. S<sub>x</sub>, S<sub>y</sub> and S<sub>z</sub> represent the spin components for the total system. The Fermi level is set to zero. The coordinates of the k-points are S<sub>1</sub>=(0.5,0.5,0) and S<sub>2</sub>=(-0.5,0.5,0) in direct coordinates.

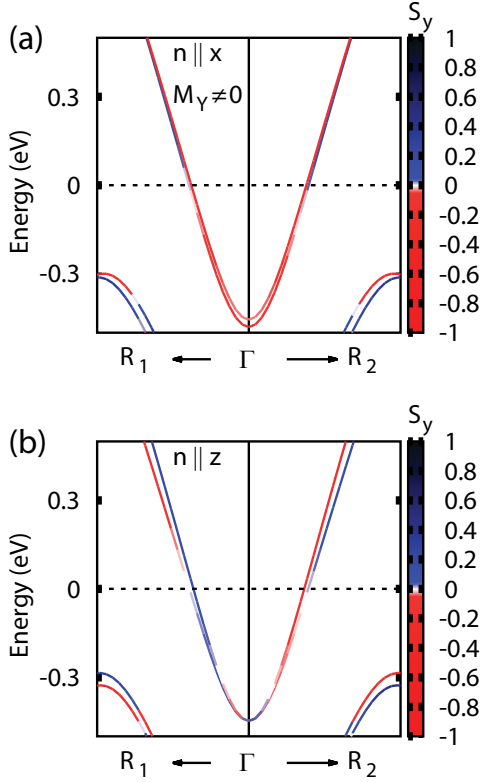


FIG. 3. Band structure of d-wave RuO<sub>2</sub> along the R<sub>1</sub>-Γ-R<sub>2</sub> low-symmetry k-path with the Néel vector along (a) the x- and (b) z-axis. The positive and negative S<sub>y</sub> and S<sub>z</sub> components are plotted in red and blue, respectively. S<sub>x</sub>, S<sub>y</sub> and S<sub>z</sub> represent the spin components for the total system. The Fermi level is set to zero. The coordinates of the k-points are R<sub>1</sub>=(0.5,0,0.5) and R<sub>2</sub>=(-0.5,0,0.5) in direct coordinates.

## II. COMPUTATIONAL DETAILS

The electronic properties were computed within the framework of density functional theory calculations based on plane wave basis set and projector augmented wave method using VASP<sup>35–37</sup> package. A plane-wave energy cut-off of 400 eV was chosen and the generalized gradient approximation of Perdew, Burke, and Ernzerhof has been used<sup>38</sup>. The Hubbard U effects for the 4d-orbitals of Ru<sup>4+</sup>, the 3d-orbitals of Cr and 3d-orbitals of Mn<sup>2+</sup> have been adopted<sup>39</sup>. We have used the value of U = 2 eV<sup>40,41</sup> keeping J<sub>H</sub> = 0.15U. The value of U strengthens the gap in MnSe and establishes a robust magnetic moment in RuO<sub>2</sub>, however, all qualitative results are independent of the value of U. We have performed the calculations using 20×20×28 and 24×24×18 k-points centered in Γ for RuO<sub>2</sub> and CrSb, respectively. A denser k-grid of 28×28×18 was used for wurtzite MnSe, which is necessary to have an accurate description of the DOS, especially in the presence of relatively small spin-orbit coupling. The lattice constants are a=4.4825 Å and c=3.1113 Å for the RuO<sub>2</sub>, a=4.103 Å and c=5.463 Å<sup>42</sup> for the CrSb and a=4.12 Å with c=6.72 Å for the MnSe<sup>43</sup>. The experimental Néel vectors are along the z-axis for RuO<sub>2</sub> and CrSb<sup>44</sup>. All calculations were performed in the presence of SOC. The information on the individual spinor components is available for the site's projected density of states in the VASP code. The site-projected orbital- and energy-resolved spin density S<sub>x</sub>, S<sub>y</sub> and S<sub>z</sub> are available. We sum over all orbitals to obtain the total S<sub>x</sub>, S<sub>y</sub> and S<sub>z</sub> components. The smearing value for the DOS was 50 meV. Regarding the magnetic space group (MSG), the RuO<sub>2</sub> has MSGs 58.398 and 136.499 for the Néel vector along the x-axis and z-axis, respectively. CrSb has MSGs 63.457, 63.462 and 194.268 for the Néel vector along the x-axis, y-axis, and z-axis, respectively. Wurtzite MnSe has the magnetic space group 194.268 when the Néel vector is along the z-axis. The

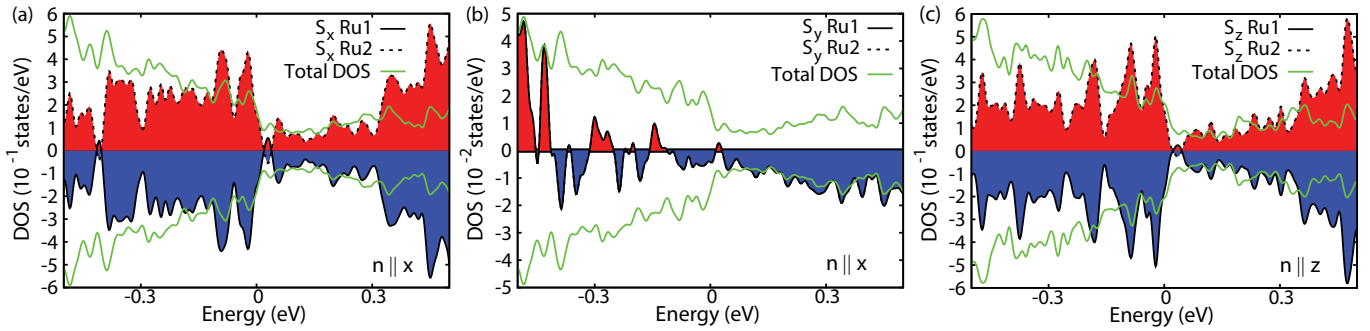


FIG. 4. DOS for the spin-components as a function of the energy for the d-wave RuO<sub>2</sub>. (a,b) DOS of the  $S_x$  and  $S_y$  components with the Néel vector along the x-axis, respectively. (c) DOS of the  $S_z$  component with Néel vector along the z-axis. The other components are antiparallel. The Fermi level is set to zero. The total DOS is plotted in green and renormalized to fit within the plot.

magnetic point group without spin-orbit coupling<sup>32,45</sup> of the wurtzite MnSe is  $6'/m'm$ , different from that of the hexagonal CrSb in the NiAs structure which is  $6'/m'm'm$ . However, both groups belong to the same magnetic Laue class ( $6'/m'm'm$ ) proving that the spin splitting of electron bands without SOC is qualitatively the same in both systems. This could be established using the formalism of spin groups<sup>6,7</sup>.

### III. RESULTS

In a centrosymmetric conventional antiferromagnet, we have Kramers degeneracy therefore the DOS of the spin-up sublattice and the spin-down sublattice are always equal for all components. The two sublattices have always antiparallel spin components and no weak ferromagnetism is possible. In a noncentrosymmetric conventional antiferromagnet with SOC, there is an additional Rashba spin-splitting where the spin components belonging to two sublattices are antiparallel.<sup>46</sup> Therefore, in noncentrosymmetric conventional antiferromagnets, there is no weak ferromagnetism as well.

We move to the study of the electronic properties responsible for weak ferromagnetism in centrosymmetric and noncentrosymmetric altermagnets. We study the electronic properties of d-wave centrosymmetric altermagnet RuO<sub>2</sub> in the first subsection. In the second and third subsections, we compare the g-wave altermagnets CrSb and wurtzite MnSe, where the former is centrosymmetric and the latter is noncentrosymmetric. We will see how SOC acts differently on centrosymmetric and noncentrosymmetric space groups. All selected compounds have two atoms per unit cell which we will call  $M_1$  and  $M_2$  ( $M = \text{Ru, Cr, Mn}$ ) to represent the properties of the two sublattices with opposite spins.

#### A. Weak ferromagnetism in centrosymmetric tetragonal altermagnet RuO<sub>2</sub>

In this subsection, we describe the metallic centrosymmetric d-wave RuO<sub>2</sub>. Several authors described the altermagnetic properties of RuO<sub>2</sub><sup>3,47</sup>, however, we will focus on the band structure and the DOS for the spin-components which were never investigated before. The appearance of the weak ferromagnetism derives from the breaking of the time-reversal symmetry, therefore, there is the chance for the spins to be not antiparallel when SOC is included. The self-consistent DFT calculations provide the energetic ground state for the parallel or antiparallel configuration of the spin components orthogonal to the Néel vector. Since RuO<sub>2</sub> is metallic, we expect that this weak ferromagnetism could be observed in the DFT calculations. Indeed, the magnetic moment orthogonal to the Néel vector is  $0.022 \mu_B$  per Ru atom along the y-axis when the Néel vector is along the x-axis. In Figs. 2 and 3, we report the band structures of RuO<sub>2</sub> projected on different spin components for the two inequivalent directions of the Néel vector (x-axis and z-axis) along the  $S_1$ - $\Gamma$ - $S_2$  and  $R_1$ - $\Gamma$ - $R_2$  low-symmetry k-paths, respectively. When the Néel vector is along the x-axis, the  $S_x$  spin component of the total system for every energy has a value along  $S_1$ - $\Gamma$  and an equal but opposite value along  $\Gamma$ - $S_2$  as reported in Fig. 2(a). As a result, the magnetization component  $M_x$  of the entire system that is the integral over the energy up to the Fermi level of  $S_x$  is always zero. On the contrary, the spin components  $S_y$  of the total system show a band structure where the value of  $S_y$  along  $S_1$ - $\Gamma$  is equal to the value along  $\Gamma$ - $S_2$ . For every value of the energy, the value of the magnetization  $M_y$  as integral of  $S_y$  will be in general non-zero resulting in a weak magnetization in the y-direction as we can see from Figs. 2(b) and 3(a). The origin of the canted spin moment derives exclusively from the spin-orbit coupling but this picture is equivalent to the DMI picture. In the case of RuO<sub>2</sub> with spins along the z-axis, we have a pure antiparallel order without weak ferromagnetism, as shown in Figs. 2(c) and 3(b). The other results were not

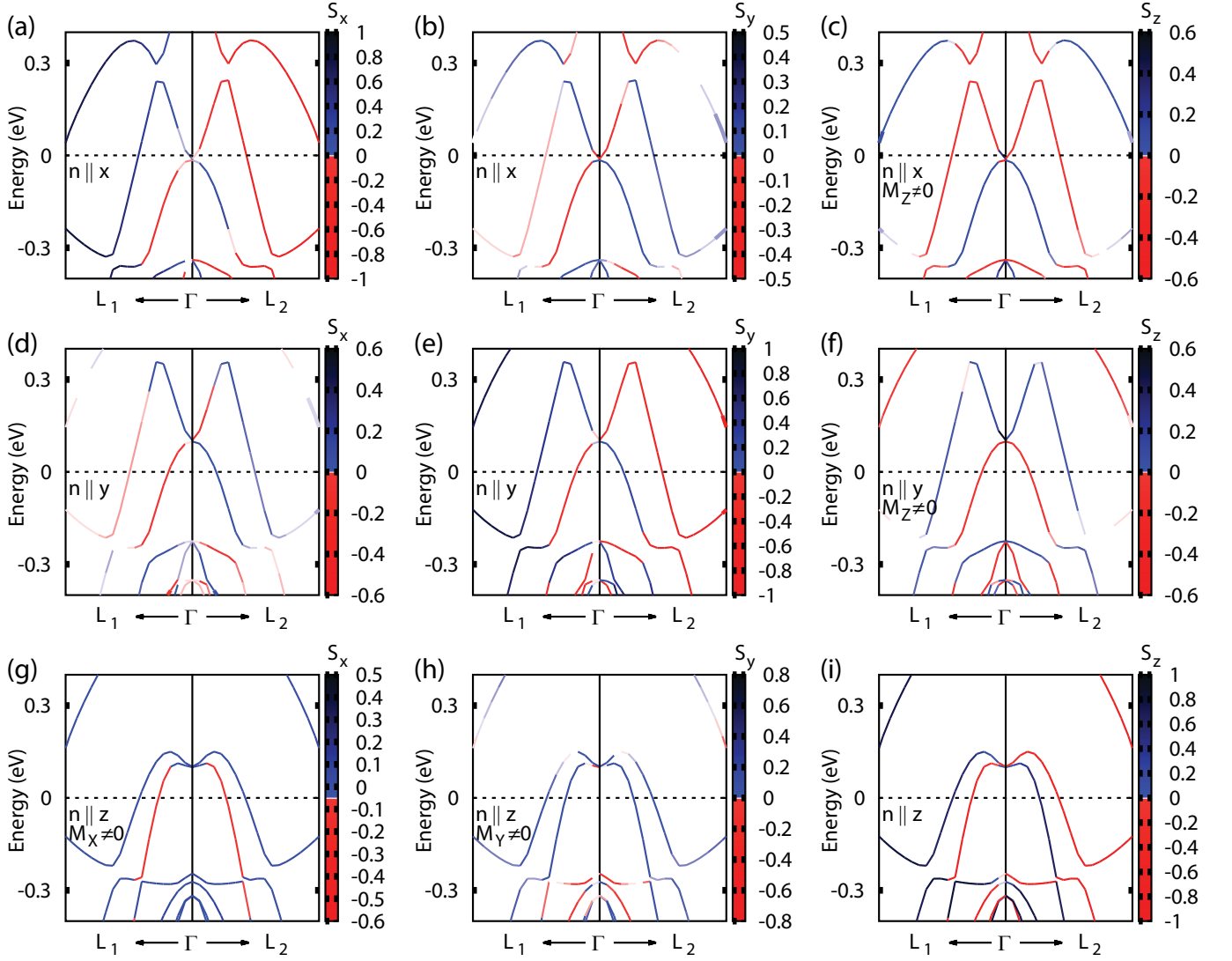


FIG. 5. Band structure of centrosymmetric CrSb with SOC along the  $L_1$ - $\Gamma$ - $L_2$  low-symmetry k-path. With the Néel vector along the x-axis, we report the projection of the spin-component (a)  $S_x$ , (b)  $S_y$  and (c)  $S_z$ . With the Néel vector along the y-axis, we report the projection of the spin-component (d)  $S_x$ , (e)  $S_y$  and (f)  $S_z$ . With the Néel vector along the z-axis, we report the projection of the spin-component (g)  $S_x$ , (h)  $S_y$  and (i)  $S_z$ .  $S_x$ ,  $S_y$  and  $S_z$  represent the spin components for the total system. The Fermi level is set to zero. The coordinates of the k-points are  $L_1=(0.5,0,0.5)$  and  $L_2=(-0.5,0,0.5)$  in direct coordinates.

shown because they are either equivalent to the shown results or with null spin components. The band degeneracy is broken at  $\Gamma$  for the Néel vector along the x-axis, but not for the Néel vector along to z-axis. Therefore, we have lifting of the degeneracy at  $\Gamma$  when the weak ferromagnetism rises.

To further extend our consideration to the entire Brillouin zone, we also show the density of states for the non-zero and inequivalent spin components in Fig. 4 for the Néel vector along the x- and z-axis. When the Néel vector is along the x-axis, the local DOSs of the  $S_x$  components for the two sublattices are equal and opposite as described by the local DOS related to atoms  $Ru_1$  and  $Ru_2$  in Fig. 4(a), therefore, the  $S_x$  components are equal and

opposite for the two sublattices. From the DOS of the  $S_y$  component reported in 4(b), it is further clear that there is a magnetic moment along the y-axis on the  $Ru_1$  and  $Ru_2$  atoms that are equal and in the same direction resulting in a weak ferromagnetism. The DOSs of the spin component  $S_y$  for the atoms  $Ru_1$  and  $Ru_2$  are perfectly equal, therefore, the size of the local magnetic moments of  $Ru_1$  and  $Ru_2$  are equal as expected since the two atoms are connected by roto-translation symmetries. We can see that we have a sign change in  $M_y$  as a function of the energy, this could be accompanied by a sign change of the AHE. Comparing the DOS of the spin-component  $S_x$  with the total DOS, we can see a strong reduction of  $S_x$  around -0.4 eV together with the maximum of  $S_y$ ,

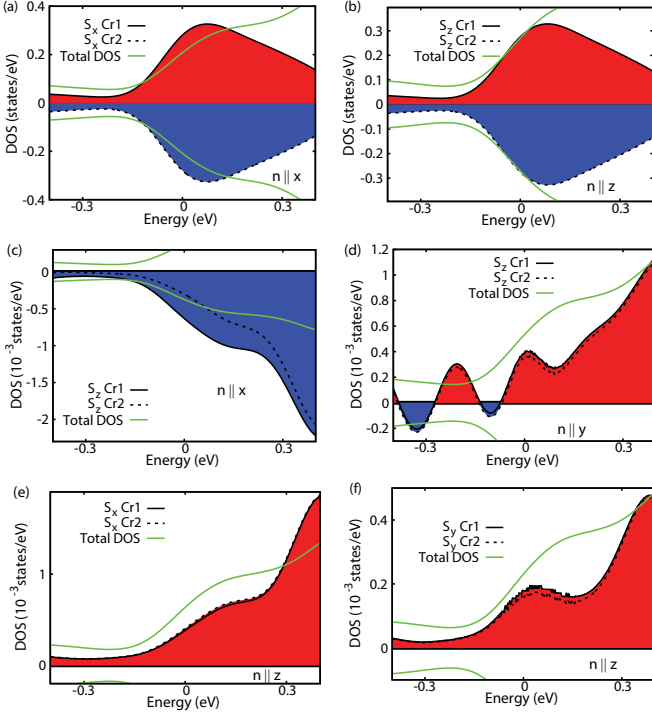


FIG. 6. DOS for the spin-components  $S_x$ ,  $S_y$  and  $S_z$  as a function of the energy for the centrosymmetric CrSb. (a,b) DOS for the components  $S_x$  and  $S_z$  with the Néel vector along the x-axis and along the z-axis, respectively. (c,d) DOS for the spin component  $S_z$  with the Néel vector along the x-axis and along the y-axis, respectively. Both of them show weak ferromagnetism. (e,f) DOS for the spin component  $S_x$  and  $S_y$  with the Néel vector along the z-axis. Both of them show weak ferromagnetism. The Fermi level is set to zero. The total DOS is renormalized to fit within the plot.

therefore, there is a strong rotation of the  $S_x$  component into the  $S_y$  component at  $-0.4$  eV. In the case of the Néel vector along the z-axis, the DOS of all spin-components relative to  $\text{Ru}_1$  and  $\text{Ru}_2$  are equal and opposite, therefore, the Ru spins are perfectly compensating each other as it is shown in Fig. 4(c), consequently, there is no weak ferromagnetism. From the DOS we can also understand that the system presents ferromagnetic or antiferromagnetic features depending on the orientation of the Néel vector, and this property in the k-space is the same in the whole Brillouin zone and for all bands.

### B. Weak ferromagnetism in centrosymmetric hexagonal altermagnet CrSb

We repeat the investigation for the g-wave centrosymmetric altermagnet CrSb. In Figs. 5, we report the band structures of CrSb projected on different spin components ( $S_x$ ,  $S_y$  and  $S_z$ ) for the three different directions of the Néel vector along the  $L_1$ - $\Gamma$ - $L_2$  focusing on the region near  $\Gamma$  point. The ground state is altermagnetic phase with the Néel vector along the z-axis, we have an energy

difference of 0.2 meV per formula unit with respect to the in-plane Néel vector. When the Néel vector is along the x-axis as in Fig. 5(a,b,c), we have weak ferromagnetism only for  $S_z$  resulting in a non-zero value of  $M_z$ . We have qualitatively similar results when the Néel vector is along the y-axis as in Fig. 5(d,e,f). We have weak ferromagnetism only for  $S_z$  resulting in a non-zero value of  $M_z$ . When we have the Néel vector along the z-axis, we have weak ferromagnetism for the  $S_x$  and  $S_y$  components resulting in a non-zero  $M_x$  and  $M_y$  as shown in 5(g,h,i). Overall, we find a weak ferromagnetism out-of-plane when the Néel vector is in-plane and a weak ferromagnetism in-plane when the Néel vector is out-of-plane. Additionally, we find a strong change in the relativistic band structure as a function of the Néel vector, especially between in-plane and out-of-plane directions of the Néel vector. Qualitatively similar results are observed for the high-symmetry k-path  $K_1$ - $\Gamma$ - $K_2$  (not reported) with the difference that  $S_z$  is always zero when the Néel vector is along the z-axis since the non-relativistic spin splitting is absent. We check the electronic properties in the DOS as well where we have information along the entire Brillouin zone and not for a limited number of k-points. The DOS for  $S_x$  and  $S_z$  when the Néel vector is along the x- and z-axis are reported in 6(a) and (b), respectively. We compare the DOS of the spin components with the total DOS illustrated in green. At energy 0.2 eV above the Fermi level, the spin-component resolved DOS with spin along the Néel vectors has less weight with respect to the total DOS. This could mean that 0.2 eV above the Fermi level there is DOS from non-magnetic atoms or there is a rotation of the spins with the weight of the DOS moving towards the spin components orthogonal to the Néel vector. When the Néel vector is along the x- and y-axis, we have non-zero magnetization along the z-axis. The values of DOS for  $S_z$  are reported in 6(c) and (d) for the Néel vector along the x- and y-axis. The case with Néel vector along the x-axis gives the larger weak ferromagnetism for CrSb with a value of  $-0.002 \mu_B$  per formula unit. We can observe a value of the total DOS above 0.2 eV larger than the DOS of the spin-component, therefore, the spins in this region are rotated from the main component by spin-orbit. We can see that the DOS of  $S_z$  is positive or negative depending on whether the Néel is along the y- or x-axis. This means that by rotating the Néel vector in the xy plane, we will have a sign change of  $M_z$ . This sign change of  $M_z$  could also produce a sign change of the anomalous Hall effect. Recent studies on the sign change of the AHE in ferromagnets have explained this effect which is relatively rare in experimental conditions<sup>48,49</sup>. When the Néel vector is along the z-axis, we observe weak ferromagnetism for both spin components for  $S_x$  and  $S_y$  reported in 6(e) and (f).

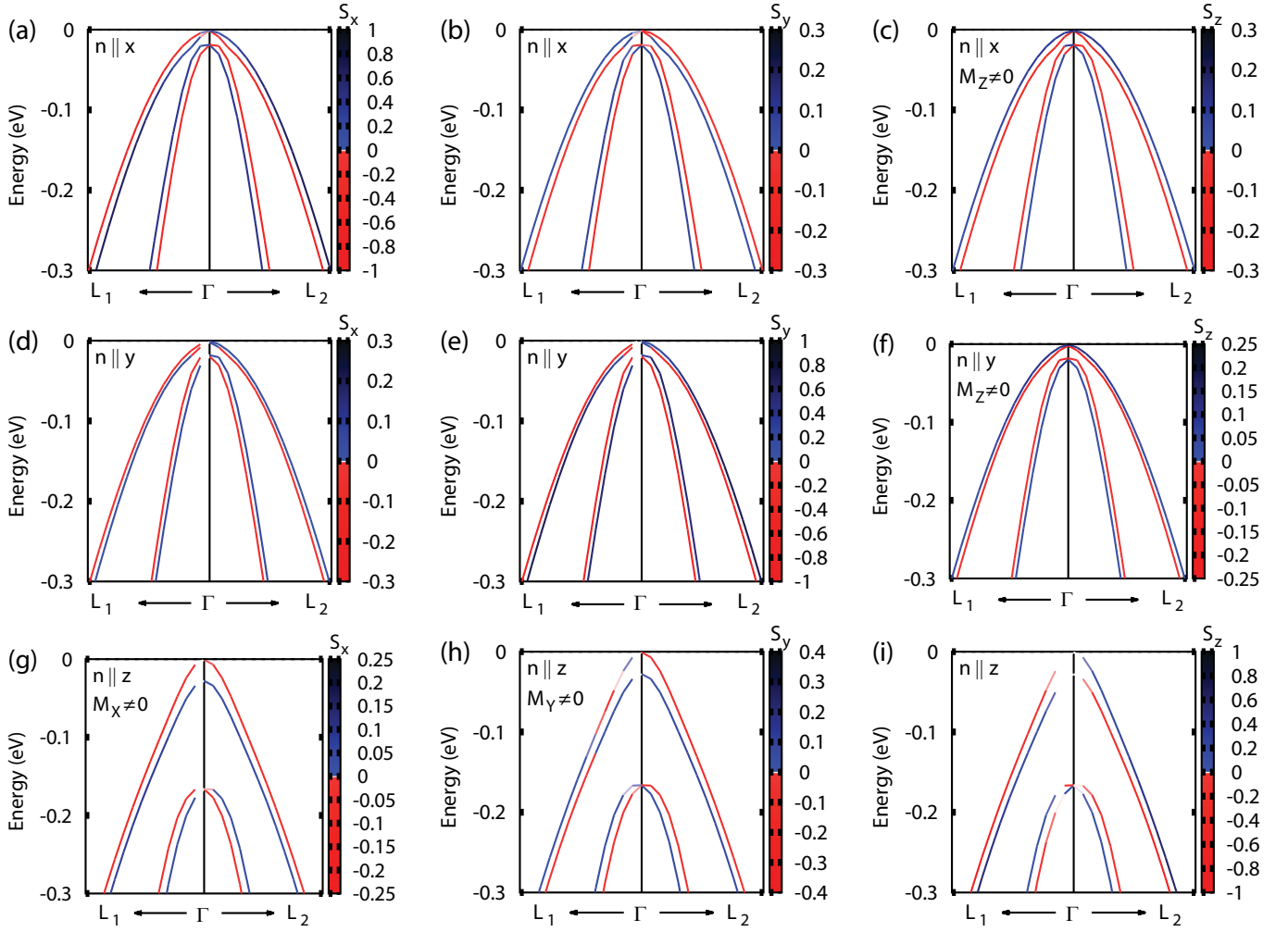


FIG. 7. Band structure of noncentrosymmetric MnSe with SOC along the  $L_1$ - $\Gamma$ - $L_2$  low-symmetry k-path. With the Néel vector along the x-axis, we report the projection of the spin-component (a)  $S_x$ , (b)  $S_y$  and (c)  $S_z$ . With the Néel vector along the y-axis, we report the projection of the spin-component (d)  $S_x$ , (e)  $S_y$  and (f)  $S_z$ . With the Néel vector along the z-axis, we report the projection of the spin-component (g)  $S_x$ , (h)  $S_y$  and (i)  $S_z$ .  $S_x$ ,  $S_y$  and  $S_z$  represent the spin components for the total system. The Fermi level is set to zero. The coordinates of the k-points are  $L_1=(0.5,0,0.5)$  and  $L_2=(-0.5,0,0.5)$  in direct coordinates.

### C. Weak FM and Weak ferrimagnetism in noncentrosymmetric hexagonal altermagnet MnSe

To understand the effect of the breaking of the inversion symmetry, we analyze MnSe which is a hexagonal g-wave altermagnet like CrSb. Indeed, MnSe with a wurtzite crystal structure represents the case of an altermagnet without inversion symmetry with a small number of atoms in the unit cell. The structural and electronic properties without SOC for wurtzite MnSe are reported in the literature<sup>43</sup>. The non-relativistic spin-splitting in wurzite MnSe can reach a maximum of 200-300 meV in the Mn-bands, the SOC of Mn is of the order of 30 meV while the SOC of Se is 140 meV. Therefore, the SOC would be a perturbation at least in the region where the spin-splitting is maximum. For MnSe, the top of the valence band at  $\Gamma$  and A are mainly  $p_x/p_y$  with a sizeable

contribution from Mn orbitals. When the Néel vector is moved from in-plane to out-of-plane, the top of the valence band rises. We have a reduction of the band gap of 80 meV (from 1.72 to 1.64 eV) when we move from AFM with the Néel vector in the plane to AFM with the Néel vector out-of-plane. The same sensitivity of the band gap from the Néel vector was found for the centrosymmetric g-wave altermagnet MnTe.<sup>50</sup>

We calculate the band structure for the three different spin components along the low symmetry k-path  $L_1$ - $\Gamma$ - $L_2$  where we have the non-relativistic spin-splitting. The top of the valence band at the  $\Gamma$  point without SOC is four-fold degenerate. Starting from the low-symmetry k-path  $L_1$ - $\Gamma$ - $L_2$  reported in Fig. 7, we find a relativistic spin-splitting in all cases. When the Néel vector is in the plane, the eigenvalues at the  $\Gamma$  point split into two eigenvalues twofold degenerate with zero magnetization

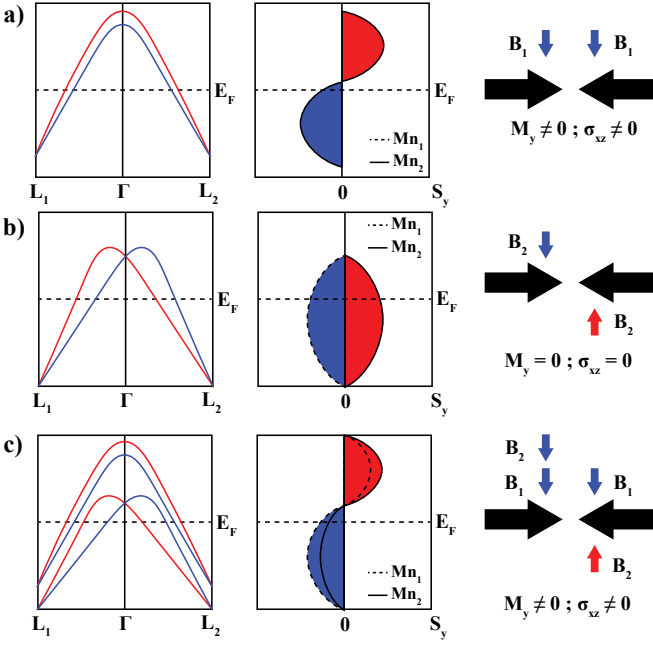


FIG. 8. Schematic band structure of noncentrosymmetric altermagnets with Néel vector along the z-axis. The red and blue colors represent the negative and positive  $S_y$  components of the total system in the band structure. DOS of the spin component  $S_y$  and magnetic configuration for three selected cases. a) Weak ferromagnetism in some bands (B1) of noncentrosymmetric altermagnets. b) Weak antiferromagnetism in some bands (B2) of noncentrosymmetric altermagnets. c) Weak ferrimagnetism as the superposition of weak FM and weak AFM from bands B1 and B2.

in the plane (see Figs. 7(a,b,d,e)) and non-zero magnetization along the z-axis (see Figs. 7(c,f)). When the Néel vector is along the z-axis, there is a strong splitting with the two highest eigenvalues single-degenerate and the one eigenvalue double-degenerate at the  $\Gamma$  point. The single-degenerate highest eigenvalues produce non-zero  $M_x$  and  $M_y$  as shown in Fig. 7(g) and 7(h), respectively. However, the double degenerate bands show antiparallel spin components. Without SOC, there is a fourfold degeneracy in the top of the valence band<sup>43</sup>. When the system is noncentrosymmetric as in the wurzite structure, we can have a combination of parallel and antiparallel spin orientation despite both sets of bands coming from the same fourfold degenerate point without SOC. As a consequence in the DOS, we will see that we do not have a completely parallel or antiparallel DOS weight. Finally, 7(i) shows the sign and weight of  $S_z$  on the two sublattices that are equal and opposite when the Néel vector is along the z-axis. Qualitatively similar results are observed for the  $K_1$ - $\Gamma$ - $K_2$  path (not reported) with the difference that  $S_z$  is always zero when the Néel vector is along the z-axis since the non-relativistic spin splitting is absent. We find weak ferromagnetism for g-wave compounds along the same direction with or without inversion symmetry. The main difference is the coexistence of

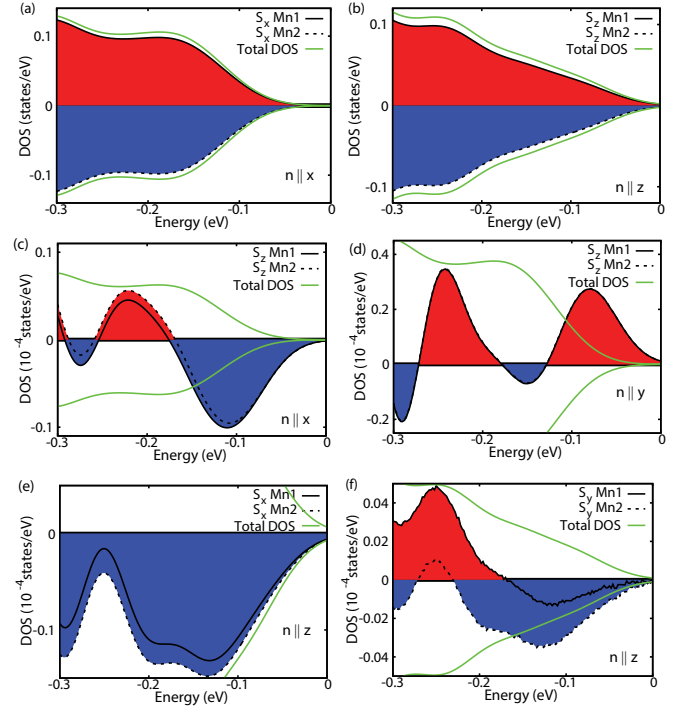


FIG. 9. DOS for the spin-components  $S_x$ ,  $S_y$  and  $S_z$  as a function of the energy for the wurzite MnSe. (a,b) DOS for the spin components  $S_x$  and  $S_z$  with the Néel vector along the x-axis and along the z-axis, respectively. (c,d) DOS for the spin component  $S_z$  with the Néel vector along the x-axis and along the y-axis, respectively. (e,f) DOS for the spin component  $S_x$  and  $S_y$  with the Néel vector along the z-axis, respectively. The solid and dashed lines represent the local spin components  $S_x$ ,  $S_y$  and  $S_z$  for the two sublattices represented by Mn1 and Mn2. The Fermi level is set to zero. The total DOS is renormalized to fit within the plot.

both parallel and antiparallel magnetic configurations for the different bands of the in-plane spin-components when the Néel is along the z-axis. Basically, we have the superposition of weak ferromagnetism [see Fig. 8](a) and weak antiferromagnetism [see Fig. 8](b)]. The superposition of both kinds of magnetism as reported schematically in Fig. 8(c) ends up forming weak ferrimagnetism (weak FiM). In this case, there is no exact compensation of the magnetization along the Néel vector and the Hall vector has a component along the Néel vector too.

To further check the results from the band structure, we report in Fig. 9 the resolved DOS for the spin-sublattice and spin components  $S_x$ ,  $S_y$  and  $S_z$  for different directions of the Néel vector, namely along the x-, y- and z-axis. The DOSs for the spin components along the Néel vector are reported in Fig. 9(a,b). The two sublattices, represented by the Mn1 and Mn2 local DOS, have equal and opposite DOS of the spin components since the spins are antiparallel. Summing the DOSs of the components along the Néel vector for the two sublattices, we would obtain zero. Now, we focus on the components orthogonal to the Néel vector. The size of

these DOSs is 3-4 orders of magnitude smaller than the size of the DOSs for the spin-components along the Néel vector. When the Néel vector is along the x-axis, we observe from Fig. 9(a,c) that the in-plane  $S_x$  components of the two sublattices are antiparallel, while the spin components  $S_z$  are parallel. Since the filling was completed and the MnSe is an insulator, the weak ferromagnetism was not obtained in the computational details but in the case of p-doping, the weak ferromagnetism would be observable. Assuming a p-doping, the magnetization  $M_z$  obtained integrating the spin density up to the Fermi level will be non-zero and the system will host a weak ferromagnetism along the z-direction. The same happens for the Néel vector along the y-axis, the in-plane components are antiparallel while we have weak ferromagnetism along  $S_z$  as shown in Fig. 9(d). When the Néel vector is along the z-axis, we have both  $M_x$  and  $M_y$  components different from zero, as shown in Fig. 9(e,f). When the Néel vector is in the xy plane, the weak ferromagnetism is along the z-axis. When the Néel vector is along the z-axis, the weak ferromagnetism is in the xy plane. This weak ferromagnetism generates AHE with the Hall vector along the direction of the weak ferromagnetism. We observe that the Hall vector is always orthogonal to the Néel vector. Even if some band structures resemble the Rashba-like dispersions, the spin textures of the altermagnets are different and more complicated than the Rashba effect<sup>9</sup>. Of course, a Rashba spin texture rises on top of the altermagnetic spin texture when the system lacks inversion symmetry like in the wurtzite structure. For the wurtzite with Néel vector along the z-axis, we have a coexistence of bands with parallel and antiparallel components regarding  $S_x$  and  $S_y$  as shown in Fig. 7(g) and (h), respectively.

#### IV. DISCUSSION AND CONCLUSIONS

In this paper, we propose that all compounds hosting weak ferromagnetism induced by the relativistic Dzyaloshinskii-Moriya interaction<sup>18,19</sup> belong to the family of the altermagnets. While Dzyaloshinskii and Moriya focused on the interplay between magnetic interactions and symmetries, the recent studies on altermagnetism provided a deeper knowledge of the crystal symmetries, extended the investigation on the magnetic properties and discovered new effects on the electronic properties<sup>1,4-7,33</sup>. The connection between these two fields emphasized in this paper paves the way to simplify the physical scenario and merge the two fields giving the chance to connect the literature developed from two different perspectives which until now had a minor overlap.

In Table I, we report several altermagnetic compounds with different space groups where the non-relativistic spin-splitting and the weak ferromagnetism were theoretically predicted or experimentally detected. All the compounds described in the seminal papers of Dzyaloshinskii and Moriya are altermagnets present in this table<sup>19</sup>.

Compound (No. space group)	NO SOC splitting	Weak FM from DMI
(Sr,Ca) <sub>3</sub> Ru <sub>2</sub> O <sub>7</sub> (36)	-	Exp. <sup>51</sup>
Ca <sub>3</sub> Mn <sub>2</sub> O <sub>7</sub> (36)	Th. <sup>9</sup>	Exp. <sup>52</sup>
Mn(N(CN) <sub>2</sub> ) <sub>2</sub> (58)	Th. <sup>9</sup>	Exp. <sup>53</sup>
Ca <sub>2</sub> RuO <sub>4</sub> (61)	Th. <sup>54</sup>	-
YVO <sub>3</sub> (62)	Th. <sup>54</sup>	Exp. <sup>55</sup>
LaMnO <sub>3</sub> (62)	Th. <sup>56</sup>	Exp. <sup>57</sup>
CaMnO <sub>3</sub> (62)	Th. <sup>9</sup>	Exp. <sup>58</sup>
YCrO <sub>3</sub> (62)	Th. <sup>9</sup>	Exp. <sup>59</sup>
CaCrO <sub>3</sub> (62)	Th. <sup>60</sup>	Th. <sup>60</sup>
Ba <sub>2</sub> CoGe <sub>2</sub> O <sub>7</sub> (113)	Th. <sup>9</sup>	Exp. <sup>61</sup>
RuO <sub>2</sub> (136)	Th. <sup>6</sup>	Th. <sup>*</sup> , Exp. <sup>47</sup>
La <sub>2</sub> NiO <sub>4</sub> (138)	Th. <sup>9</sup>	Exp. <sup>62</sup>
LiFeP <sub>2</sub> O <sub>7</sub> (140)	Th. <sup>9</sup>	Exp. <sup>63</sup>
KMnF <sub>3</sub> (140)	Th. <sup>9</sup>	Exp. <sup>64</sup>
MnTiO <sub>3</sub> (161)	Th. <sup>9</sup>	Exp. <sup>65</sup>
$\alpha$ -Fe <sub>2</sub> O <sub>3</sub> (167)	Th. <sup>9</sup>	Th. <sup>19</sup> , Exp. <sup>66</sup>
MnCO <sub>3</sub> (167)	Th. <sup>9</sup>	Th. <sup>19</sup> , Exp. <sup>67</sup>
CoCO <sub>3</sub> (167)	Th. <sup>9</sup>	Th. <sup>19</sup> , Exp. <sup>68</sup>
CrF <sub>3</sub> (167)	Th. <sup>9</sup>	Th. <sup>19</sup> , Exp. <sup>69</sup>
CoF <sub>3</sub> (167)	Th. <sup>9</sup>	Exp. <sup>70</sup>
FeF <sub>3</sub> (167)	Th. <sup>9</sup>	Exp. <sup>70</sup>
FeBO <sub>3</sub> (167)	Th. <sup>9</sup>	Exp. <sup>71</sup>
Ni <sub>1/3</sub> NbS <sub>2</sub> (182)	Th. <sup>72</sup>	-
Ni <sub>1/3</sub> TaS <sub>2</sub> (182)	Th. <sup>72</sup>	-
MnSe (186)	Th. <sup>43</sup>	Th. <sup>*</sup>
MnTe (194)	Th. <sup>6</sup> , Exp. <sup>73</sup>	Th. <sup>74</sup> , Exp. <sup>74</sup>
CrSb (194)	Th. <sup>6</sup> , Exp. <sup>42</sup>	Th. <sup>*</sup> , Exp. <sup>75</sup>

\* Present work.

TABLE I. List of selected altermagnetic compounds where the non-relativistic spin-splitting appears with weak ferromagnetism induced by DMI. The words "Th." and "Exp." are reported for the theoretical and experimental verification of the non-relativistic spin splitting or weak ferromagnetism. The space groups 36, 182 and 186 lack inversion symmetry.

Due to the lifting of the Kramers degeneracy, all altermagnetic systems could potentially show weak ferromagnetism, however, for particular Néel vector orientations the DMI is zero as in the case of the RuO<sub>2</sub> with Néel vector along the z-axis. Once separating the centrosymmetric and noncentrosymmetric compounds, we propose to divide the centrosymmetric altermagnets into two classes as shown in Fig. 10. The g-wave CrSb falls into the first category which exhibits weak ferromagnetism for every Néel vector. In the second category, are some altermagnets that do not display weak ferromagnetism for a given Néel vector, such as the d-wave CaCrO<sub>3</sub><sup>60</sup> and RuO<sub>2</sub> where we have shown that the Néel vector is oriented along the z-axis. In the DMI picture, the symmetries do not allow the presence of the DMI vector for particular Néel vector orientation. The compounds belonging to this second class are probably a limited number and seem to have higher symmetry with respect to the first

class. As a consequence of this proposed classification, the family of altermagnets is wider than the family of weak ferromagnets since there are altermagnets that do not exhibit weak ferromagnetism. For the noncentrosymmetric systems, we have found that weak FM or weak FiM are present depending on the Néel vector orientation. To extend this classification, further studies are needed especially for the noncentrosymmetric systems. In this prospect, interesting compounds are the metallic d-wave  $\text{Ca}_3\text{Ru}_2\text{O}_7$  and the metallic g-wave  $\text{Ni}_{1/3}\text{MS}_2$  ( $\text{M}=\text{Nb}, \text{Ta}$ ). These results will be presented elsewhere.

Beyond the crystal symmetries and the Néel vector orientation, the only other requirement for weak FM or weak FiM is to have a non-compensated magnetization as happens in metallic systems or doped semiconductors. As shown in Fig. 1, when the system is insulating no weak ferromagnetism is observable since there is a spin compensation, therefore, a small doping is necessary as in the case of  $\text{MnTe}$ <sup>74</sup> and other semiconductive altermagnets. From the DOS of the spin-components, we can understand that doping can change the Fermi level, strongly modify the weak ferromagnetism, and can even reverse the sign of the DMI. This explains the dependence of the weak ferromagnetism from electron- or hole-doping concentration in several cases<sup>76,77</sup>. What was defined as "weak altermagnetism" is the band structure effect that gives rise to the DMI in centrosymmetric altermagnets.<sup>73</sup> The electric field increases or activates the non-relativistic spin-splitting depending on the field orientation<sup>56,78</sup>, therefore, the electric field can increase and manipulate the DMI in altermagnets<sup>79</sup>. We can make another observation regarding centrosymmetric altermagnetic systems that can host an active DMI. In the case of magnetic systems with frustrated magnetic interactions, the presence of an active DMI in altermagnetic crystal structure can further push the system towards helical magnetic structures, spin spiral and complex magnetism as observed for instance in transition metal mononitrides<sup>80,81</sup>. The component of the weak ferromagnetism is proportional to the spin-orbit, therefore, to look for a large canting angle we need to search among systems with a strong spin-orbit and a small magnetic moment. In the weak ferromagnets, an extremely relevant role is given by the magnetocrystalline anisotropy (MCA) that decides a key ingredient as the direction of the Néel vector. Additionally, the size of the MCA determines how easy it is for the spin to rotate, therefore a low MCA is fundamental to favor the weak ferromagnetism. Even if there are altermagnets where the weak ferromagnetism is zero in the bulk as the compounds belonging to the second class, the weak ferromagnetism can be obtained by breaking crystal symmetries on the surfaces. Further studies are necessary for the evolution of the DMI and weak ferromagnetism on the surfaces of the altermagnets.<sup>56,82</sup>

In conclusion, we propose that weak ferromagnetism induced by DMI can appear in centrosymmetric and non-centrosymmetric altermagnetic compounds but not in

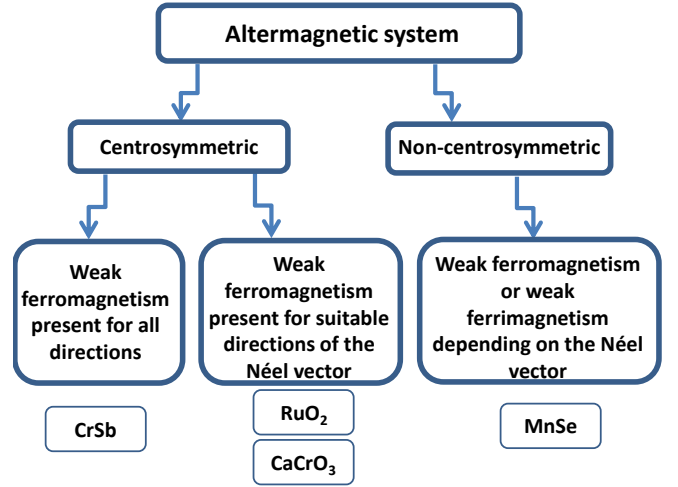


FIG. 10. Altermagnets classified into centrosymmetric and noncentrosymmetric. We further classify the centrosymmetric systems into two classes; the first contains compounds in which the weak FM is always present, and the second contains compounds in which the weak FM is present for suitable directions of the Néel vector. For the noncentrosymmetric  $\text{MnSe}$ , we have weak ferromagnetism with the Néel vector in the xy plane and weak ferrimagnetism with the Néel vector out-of-plane. Likely, this classification would be improved and extended in coming years.

centrosymmetric and noncentrosymmetric conventional antiferromagnets. Weak FiM can appear in noncentrosymmetric altermagnets. This weak ferromagnetism originates exclusively from the spin-orbit coupling in altermagnets and this picture is equivalent to the DMI picture. The weak ferromagnetism and the AHE are always orthogonal to the Néel vector for centrosymmetric systems. The weak ferromagnetism depends on the filling, can be tuned by an electric field and can change its sign by rotating the Néel vector in hexagonal systems. From our results, the weak ferromagnetism is absent for insulators and in lightly doped semiconductive systems would be proportional to the carriers. We provide a recipe to establish the presence of weak ferromagnetism and the components of the Hall vector from a simple relativistic density of state and band structure calculations without calculating the DMI vector. There is a correlation between the rise of weak FM and weak FiM with the lifting of the electronic degeneracy at the  $\Gamma$  point. We have the centrosymmetric altermagnetic and the noncentrosymmetric altermagnets. We further divided the centrosymmetric altermagnets into two classes, the first class always hosts weak ferromagnetism for every direction of the Hall vector while the other class hosts weak ferromagnetism for suitable directions of the Néel vector. For noncentrosymmetric systems, we have weak ferromagnetism in the x-y plane while parallel and antiparallel spin components for different bands can coexist at the same energy resulting in weak ferrimagnetism and a component of the Hall vector along the Néel vector. Therefore, an exter-

nal electric field breaking the inversion symmetry could generate a weak ferromagnetic component and an AHE along the Néel vector. We have predicted weak ferromagnetism in CrSb and weak ferrimagnetism in wurzite MnSe. The size of weak ferromagnetism, weak ferrimagnetism and AHE strongly depends on the spin-orbit coupling, therefore, further research directions should focus on heavy elements. In summary, the family of the altermagnets is mainly composed of weak ferromagnets with a minor number of compounds that are weak ferrimagnets (MnSe with Néel vector along the z-axis) and zero magnetization compounds (RuO<sub>2</sub> with Néel vector along the z-axis). It was shown that altermagnetism displays properties that either belong to ferromagnets or conventional antiferromagnets<sup>1</sup>, the weak FM and weak FIM induced by DMI are properties belonging exclusively to altermagnets not present neither in ferromagnets or in conventional antiferromagnets. If we want to classify altermagnets based on their macroscopic physical properties, we can define altermagnets as magnetic systems with spin-up and spin-down sublattices connected by symmetry where the DMI allows the rise of weak ferromagnetism for a suitable Néel vector orientation.

## ACKNOWLEDGMENTS

C. A., R. M. S. and G. C. contributed equally to this work. We acknowledge M. Cuoco, K. Výborný, M. Gryglas-Borysiewicz and M. Grzybowski for useful discussions. The work is supported by the Foundation for Polish Science through the International Research Agendas program co-financed by the European Union within the Smart Growth Operational Programme (Grant No. MAB/2017/1). A.F. was supported by the Polish National Science Centre under project no. 2020/37/B/ST5/02299. We acknowledge the access to the computing facilities of the Interdisciplinary Center of Modeling at the University of Warsaw, Grant g91-1418, g91-1419 and g91-1426 for the availability of high-performance computing resources and support. We acknowledge the CINECA award under the ISCRA initiative IsC99 "SILENTS", IsC105 "SILENTSG" and IsB26 "SHINY" grants for the availability of high-performance computing resources and support. We acknowledge the access to the computing facilities of the Poznan Supercomputing and Networking Center Grant No. 609.

\* autieri@magtop.ifpan.edu.pl

† rsattigeri@magtop.ifpan.edu.pl

‡ gcuono@magtop.ifpan.edu.pl

<sup>1</sup> Igor Mazin *et al.*, "Altermagnetism—a new punch line of fundamental magnetism," *Physical Review X* **12**, 040002 (2022).

<sup>2</sup> Carmine Autieri, "In manuscript," (2024).

<sup>3</sup> Libor Šmejkal, Rafael González-Hernández, T. Jungwirth, and J. Sinova, "Crystal time-reversal symmetry breaking and spontaneous hall effect in collinear antiferromagnets," *Science Advances* **6**, eaaz8809 (2020), <https://www.science.org/doi/pdf/10.1126/sciadv.aaz8809>.

<sup>4</sup> Satoru Hayami, Yuki Yanagi, and Hiroaki Kusunose, "Momentum-dependent spin splitting by collinear antiferromagnetic ordering," *Journal of the Physical Society of Japan* **88**, 123702 (2019).

<sup>5</sup> Satoru Hayami, Yuki Yanagi, and Hiroaki Kusunose, "Bottom-up design of spin-split and reshaped electronic band structures in antiferromagnets without spin-orbit coupling: Procedure on the basis of augmented multipoles," *Physical Review B* **102**, 144441 (2020).

<sup>6</sup> Libor Šmejkal, Jairo Sinova, and Tomas Jungwirth, "Emerging research landscape of altermagnetism," *Phys. Rev. X* **12**, 040501 (2022).

<sup>7</sup> Libor Šmejkal, Jairo Sinova, and Tomas Jungwirth, "Beyond conventional ferromagnetism and antiferromagnetism: A phase with nonrelativistic spin and crystal rotation symmetry," *Phys. Rev. X* **12**, 031042 (2022).

<sup>8</sup> Lin-Ding Yuan and Alex Zunger, "Degeneracy removal of spin bands in collinear antiferromagnets with non-interconvertible spin-structure motif pair," *Advanced Materials*, 2211966 (2023).

<sup>9</sup> Yaqian Guo, Hui Liu, Oleg Janson, Ion Cosma Fulga, Jeroen van den Brink, and Jorge I. Facio, "Spin-split

collinear antiferromagnets: A large-scale ab-initio study," *Materials Today Physics* **32**, 100991 (2023).

<sup>10</sup> Giuseppe Cuono, Raghottam M. Sattigeri, Carmine Autieri, and Tomasz Dietl, "Ab initio overestimation of the topological region in eu-based compounds," *Phys. Rev. B* **108**, 075150 (2023).

<sup>11</sup> Rafael González-Hernández, Libor Šmejkal, Karel Výborný, Yuta Yahagi, Jairo Sinova, Tomáš Jungwirth, and Jakub Železný, "Efficient electrical spin splitter based on nonrelativistic collinear antiferromagnetism," *Phys. Rev. Lett.* **126**, 127701 (2021).

<sup>12</sup> Libor Šmejkal, Anna Birk Hellenes, Rafael González-Hernández, Jairo Sinova, and Tomas Jungwirth, "Giant and tunneling magnetoresistance in unconventional collinear antiferromagnets with nonrelativistic spin-momentum coupling," *Phys. Rev. X* **12**, 011028 (2022).

<sup>13</sup> Ding-Fu Shao, Shu-Hui Zhang, Ming Li, Chang-Beom Eom, and Evgeny Y. Tsymbal, "Spin-neutral currents for spintronics," *Nature Communications* **12** (2021), 10.1038/s41467-021-26915-3.

<sup>14</sup> Arnab Bose, Nathaniel J. Schreiber, Rakshit Jain, Ding-Fu Shao, Hari P. Nair, Jiaxin Sun, Xiyue S. Zhang, David A. Muller, Evgeny Y. Tsymbal, Darrell G. Schlom, and Daniel C. Ralph, "Tilted spin current generated by the collinear antiferromagnet ruthenium dioxide," *Nature Electronics* **5** (2022), 10.1038/s41928-022-00744-8.

<sup>15</sup> Ding-Fu Shao, Yuan-Yuan Jiang, Jun Ding, Shu-Hui Zhang, Zi-An Wang, Rui-Chun Xiao, Gautam Gurung, WJ Lu, YP Sun, and Evgeny Y Tsymbal, "Néel spin currents in antiferromagnets," *Physical Review Letters* **130**, 216702 (2023).

<sup>16</sup> Xiaodong Zhou, Wanxiang Feng, Run-Wu Zhang, Libor Šmejkal, Jairo Sinova, Yuriy Mokrousov, and Yugui Yao, "Crystal thermal transport in altermagnetic RuO<sub>2</sub>,"

- (2023), arXiv:2305.01410 [cond-mat.mtrl-sci].
- 17 Jabir Ali Ouassou, Arne Brataas, and Jacob Linder, “Josephson effect in altermagnets,” (2023), arXiv:2301.03603 [cond-mat.supr-con].
  - 18 I. Dzyaloshinsky, “A thermodynamic theory of “weak” ferromagnetism of antiferromagnetics,” *Journal of Physics and Chemistry of Solids* **4**, 241–255 (1958).
  - 19 Tôru Moriya, “Anisotropic superexchange interaction and weak ferromagnetism,” *Phys. Rev.* **120**, 91–98 (1960).
  - 20 Robert E Camley and Karen L Livesey, “Consequences of the dzyaloshinskii-moriya interaction,” *Surface Science Reports*, 100605 (2023).
  - 21 Roberto Salazar-Rodriguez, Domingo Aliaga Guerra, Jean-Marc Greneche, Keith M Taddei, Noemi-Raquel Checca-Huaman, Edson C Passamani, and Juan A Ramos-Guivar, “Presence of induced weak ferromagnetism in fe-substituted yfexr1- x03 crystalline compounds,” *Nanomaterials* **12**, 3516 (2022).
  - 22 D Treves, “Magnetic studies of some orthoferrites,” *Physical Review* **125**, 1843 (1962).
  - 23 J-S Zhou, LG Marshall, Z-Y Li, X Li, and J-M He, “Weak ferromagnetism in perovskite oxides,” *Physical Review B* **102**, 104420 (2020).
  - 24 Antony B. Blake and William E. Hatfield, “Two-dimensional antiferromagnetism and weak ferromagnetism in some anilinium salts of the types a2mnc14 and a2fecl4,” *J. Chem. Soc., Dalton Trans.* (1979), 10.1039/DT9790001725.
  - 25 Vladimir Koval, Ivan Skorvanek, Juraj Durisin, Giuseppe Viola, Alexandra Kovalcikova, Peter Svec, Karel Saksl, and Haixue Yan, “Terbium-induced phase transitions and weak ferromagnetism in multiferroic bismuth ferrite ceramics,” *J. Mater. Chem. C* **5** (2017), 10.1039/C6TC04060H.
  - 26 Dan-Feng Weng, Zhe-Ming Wang, and Song Gao, “Framework-structured weak ferromagnets,” *Chem. Soc. Rev.* **40** (2011), 10.1039/C0CS00093K.
  - 27 Hemant Dixit, Jun Hee Lee, Jaron T Krogel, Satoshi Okamoto, and Valentino R Cooper, “Stabilization of weak ferromagnetism by strong magnetic response to epitaxial strain in multiferroic bifeo3,” *Scientific reports* **5**, 12969 (2015).
  - 28 Dan-Feng Weng, Zhe-Ming Wang, and Song Gao, “Framework-structured weak ferromagnets,” *Chemical Society Reviews* **40**, 3157–3181 (2011).
  - 29 Yoshinori Tokura and Naoya Kanazawa, “Magnetic skyrmion materials,” *Chemical Reviews* **121**, 2857–2897 (2020).
  - 30 R. D. Gonzalez Betancourt, J. Zubáč, R. Gonzalez-Hernandez, K. Geishendorf, Z. Šobán, G. Springholz, K. Olejník, L. Šmejkal, J. Sinova, T. Jungwirth, S. T. B. Goennenwein, A. Thomas, H. Reichlová, J. Železný, and D. Kriegner, “Spontaneous anomalous hall effect arising from an unconventional compensated magnetic phase in a semiconductor,” *Phys. Rev. Lett.* **130**, 036702 (2023).
  - 31 A. Junxiang Wu, B. Zeyang Zhang, C. Jian Liu, and D. Xiaohong Shao, “Magnetic quadratic nodal line with spin-orbital coupling in CrSb,” *Applied Physics Letters* **123**, 052407 (2023), [https://pubs.aip.org/aip/apl/article-pdf/doi/10.1063/5.0158271/18072692/052407\\_1.5.0158271.pdf](https://pubs.aip.org/aip/apl/article-pdf/doi/10.1063/5.0158271/18072692/052407_1.5.0158271.pdf).
  - 32 Ilja Turek, “Altermagnetism and magnetic groups with pseudoscalar electron spin,” *Physical Review B* **106**, 094432 (2022).
  - 33 Amar Fakhredine, Raghottam M. Sattigeri, Giuseppe Cuono, and Carmine Autieri, “Interplay between altermagnetism and nonsymmorphic symmetries generating large anomalous hall conductivity by semi-dirac points induced anticrossings,” *Phys. Rev. B* **108**, 115138 (2023).
  - 34 M. Asa, C. Autieri, R. Pazzocco, C. Rinaldi, W. Brzezicki, A. Stroppa, M. Cuoco, G. Varvaro, S. Picozzi, and M. Cantoni, “Anomalous hall effect in antiferromagnetic/nonmagnetic interfaces,” *Phys. Rev. Res.* **2**, 043394 (2020).
  - 35 G. Kresse and J. Hafner, “Ab initio molecular dynamics for liquid metals,” *Phys. Rev. B* **47**, 558–561 (1993).
  - 36 G. Kresse and J. Furthmüller, “Efficiency of ab-initio total energy calculations for metals and semiconductors using a plane-wave basis set,” *Computational Materials Science* **6**, 15–50 (1996).
  - 37 G. Kresse and J. Furthmüller, “Efficient iterative schemes for ab initio total-energy calculations using a plane-wave basis set,” *Phys. Rev. B* **54**, 11169–11186 (1996).
  - 38 John P Perdew, Kieron Burke, and Matthias Ernzerhof, “Generalized gradient approximation made simple,” *Physical review letters* **77**, 3865 (1996).
  - 39 A. I. Liechtenstein, V. I. Anisimov, and J. Zaanen, “Density-functional theory and strong interactions: Orbital ordering in mott-hubbard insulators,” *Phys. Rev. B* **52**, R5467–R5470 (1995).
  - 40 Sergey A. Ivanov, Alexander A. Bush, Adam I. Stash, Konstantin E. Kamentsev, Valerii Ya. Shkuratov, Yaroslav O. Kvashnin, Carmine Autieri, Igor Di Marco, Biplab Sanyal, Olle Eriksson, Per Nordblad, and Roland Mathieu, “Polar order and frustrated antiferromagnetism in perovskite pb2mnwo6 single crystals,” *Inorganic Chemistry* **55**, 2791–2805 (2016).
  - 41 Rabindra Basnet, Kamila M. Kotur, Milosz Rybak, Cory Stephenson, Samuel Bishop, Carmine Autieri, Magdalena Birowska, and Jin Hu, “Controlling magnetic exchange and anisotropy by nonmagnetic ligand substitution in layered mPX<sub>3</sub> (m = Ni, mn; x = S, se),” *Phys. Rev. Res.* **4**, 023256 (2022).
  - 42 Sonka Reimers, Lukas Odenbreit, Libor Smejkal, Vladimir N. Strocov, Procopios Constantinou, Anna Birk Hellenes, Rodrigo Jaeschke Ubierno, Warley H. Campos, Venkata K. Bharadwaj, Atasi Chakraborty, Thiboud Denneulin, Wen Shi, Rafal E. Dunin-Borkowski, Suvadip Das, Mathias Kläui, Jairo Sinova, and Martin Jourdan, “Direct observation of altermagnetic band splitting in crsb thin films,” (2023), arXiv:2310.17280 [cond-mat.mtrl-sci].
  - 43 Michał J. Grzybowski, Carmine Autieri, Jarosław Domagała, Cezary Krasucki, Anna Kaleta, Sławomir Kret, Katarzyna Gas, Maciej Sawicki, Rafał Bożek, Jan Sufczyński, and Wojciech Pacuski, “Wurtzite vs rock-salt mnse epitaxy: electronic and altermagnetic properties,” (2023), arXiv:2309.06422 [cond-mat.mtrl-sci].
  - 44 Jibao Yuan, Yuzhu Song, Xianran Xing, and Jun Chen, “Magnetic structure and uniaxial negative thermal expansion in antiferromagnetic crsb,” *Dalton Trans.* **49**, 17605–17611 (2020).
  - 45 Lin-Ding Yuan, Zhi Wang, Jun-Wei Luo, Emmanuel I. Rashba, and Alex Zunger, “Giant momentum-dependent spin splitting in centrosymmetric low-z antiferromagnets,” *Phys. Rev. B* **102**, 014422 (2020).
  - 46 Kunihiro Yamauchi, Paolo Barone, and Silvia Picozzi, “Bulk rashba effect in multiferroics: A theoretical prediction for bicoo3,” *Phys. Rev. B* **100**, 245115 (2019).
  - 47 Zexin Feng, Xiaorong Zhou, Libor Šmejkal, Lei Wu, Zengwei Zhu, Huixin Guo, Rafael González-Hernández, Xiaon-

- ing Wang, Han Yan, Peixin Qin, Xin Zhang, Haojiang Wu, Hongyu Chen, Ziang Meng, Li Liu, Zhengcai Xia, Jairo Sinova, Tomáš Jungwirth, and Zhiqi Liu, “An anomalous hall effect in altermagnetic ruthenium dioxide,” *Nature Electronics* **5**, 735–743 (2022).
- 48 T. C. van Thiel, W. Brzezicki, C. Autieri, J. R. Hortensius, D. Afanasiev, N. Gauquelin, D. Jannis, N. Janssen, D. J. Groenendijk, J. Fatermans, S. Van Aert, J. Verbeeck, M. Cuoco, and A. D. Caviglia, “Coupling charge and topological reconstructions at polar oxide interfaces,” *Phys. Rev. Lett.* **127**, 127202 (2021).
  - 49 Md Shahin Alam, Amar Fakhredine, Mujeeb Ahmad, P. K. Tanwar, Hung-Yu Yang, Fazel Tafti, Giuseppe Cuono, Rajibul Islam, Bahadur Singh, Artem Lynnyk, Carmine Autieri, and Marcin Matusiak, “Sign change of anomalous hall effect and anomalous nernst effect in the weyl semimetal cealsi,” *Phys. Rev. B* **107**, 085102 (2023).
  - 50 Paulo E. Faria Junior, Koen A. de Mare, Klaus Zollner, Kyo-hoon Ahn, Sigurdur I. Erlingsson, Mark van Schilf-gaarde, and Karel Výborný, “Sensitivity of the mnte valence band to the orientation of magnetic moments,” *Phys. Rev. B* **107**, L100417 (2023).
  - 51 S. Ikeda, Y. Maeno, and T. Fujita, “Weak ferromagnetism in two-dimensional bilayered  $\text{sr}_{3-x}\text{ca}_x\text{ru}_2\text{o}_7$ ,” *Phys. Rev. B* **57**, 978–986 (1998).
  - 52 Pooja Sahlot and AM Awasthi, “Uncompensated-spins induced weak ferromagnetism in  $\text{ca}_3\text{mn}_2\text{o}_7$ : Magneto-conductive and dual magneto-capacitive effects,” *Journal of Magnetism and Magnetic Materials* **493**, 165732 (2020).
  - 53 Jamie L Manson, Carmen R Kmety, Arthur J Epstein, and Joel S Miller, “Spontaneous magnetization in the  $m[n(\text{cn})_2]_2$  ( $m = \text{cr}, \text{mn}$ ) weak ferromagnets,” *Inorganic Chemistry* **38**, 2552–2553 (1999).
  - 54 Giuseppe Cuono, Raghottam M. Sattigeri, Jan Skolimowski, and Carmine Autieri, “Orbital-selective altermagnetism and correlation-enhanced spin-splitting in strongly-correlated transition metal oxides,” *Journal of Magnetism and Magnetic Materials* **586**, 171163 (2023).
  - 55 Y. Ren, T. T. M. Palstra, D. I. Khomskii, A. A. Nugroho, A. A. Menovsky, and G. A. Sawatzky, “Magnetic properties of  $\text{yvo}_3$  single crystals,” *Phys. Rev. B* **62**, 6577–6586 (2000).
  - 56 Raghottam M. Sattigeri, Giuseppe Cuono, and Carmine Autieri, “Altermagnetic surface states: towards the observation and utilization of altermagnetism in thin films, interfaces and topological materials,” *Nanoscale* **15**, 16998–17005 (2023).
  - 57 V. Skumryev, F. Ott, J. Coey, A. Anane, J. Renard, L. Pinsard-Gaudart, and A. Revcolevschi, “Weak ferromagnetism in  $\text{LaMnO}_3$ ,” *The European Physical Journal B: Condensed Matter and Complex Systems* **11**, 401–406 (1999).
  - 58 JB MacChesney, HJ Williams, JF Potter, and RC Sherwood, “Magnetic study of the manganate phases:  $\text{CaMnO}_3$ ,  $\text{Ca}_4\text{Mn}_3\text{O}_{10}$ ,  $\text{Ca}_3\text{Mn}_2\text{O}_7$ ,  $\text{Ca}_2\text{MnO}_4$ ,” *Physical Review* **164**, 779 (1967).
  - 59 V.M. Jüdin and A.B. Sherman, “Weak ferromagnetism of  $\text{ycro}_3$ ,” *Solid State Communications* **4**, 661–663 (1966).
  - 60 Thi Phuong Thao Nguyen and Kunihiko Yamauchi, “Ab initio prediction of anomalous hall effect in antiferromagnetic  $\text{cacro}_3$ ,” *Phys. Rev. B* **107**, 155126 (2023).
  - 61 T Sato, T Masuda, and K Uchinokura, “Magnetic property of  $\text{ba}_2\text{coge}_2\text{o}_7$ ,” *Physica B: Condensed Matter* **329**, 880–881 (2003).
  - 62 X Batlle, X Obradors, MJ Sayagues, M Vallet, and J Gonzalez-Calbet, “Weak ferromagnetism and magnetic interactions in  $\text{la}_2\text{nio}_4$ ,” *Journal of Physics: Condensed Matter* **4**, 487 (1992).
  - 63 K.-C. Liang, W. Zhang, B. Lorenz, Y. Y. Sun, P. S. Halasyamani, and C. W. Chu, “Weak ferromagnetism and internal magnetoelectric effect in  $\text{lifep}_2\text{o}_7$ ,” *Phys. Rev. B* **86**, 094414 (2012).
  - 64 Kh G Bogdanova, VA Golenishchev-Kutuzov, VE Leont’ev, MR Nazipov, MM Shakirzyanov, MI Kurkin, and VV Nikolaev, “Acoustic excitation of nuclear spin waves in the easy-plane antiferromagnetic material  $\text{kmnf}_3$ ,” *Journal of Experimental and Theoretical Physics* **85**, 1001–1006 (1997).
  - 65 Angel M. Arévalo-López and J. Paul Attfield, “Weak ferromagnetism and domain effects in multiferroic  $\text{linbo}_3$ -type  $\text{mntio}_3$ -ii,” *Phys. Rev. B* **88**, 104416 (2013).
  - 66 F. J. Morin, “Magnetic susceptibility of  $\alpha\text{fe}_2\text{o}_3$  and  $\alpha\text{fe}_2\text{o}_3$  with added titanium,” *Phys. Rev.* **78**, 819–820 (1950).
  - 67 EN Maslen, VA Streltsov, NR Streltsova, and N Ishizawa, “Electron density and optical anisotropy in rhombohedral carbonates. iii. synchrotron x-ray studies of  $\text{cacro}_3$ ,  $\text{mgco}_3$  and  $\text{mnco}_3$ ,” *Acta Crystallographica Section B: Structural Science* **51**, 929–939 (1995).
  - 68 A. S. BOROVNIK-ROMANOV and V.I. OZHOGIN, “Weak ferromagnetism in an antiferromagnetic  $\text{coco}_3$  single crystal,” *Acta Crystallographica Section B: Structural Science* **12**, 18–24 (1961).
  - 69 M Tamine, “Surface spin-wave spectra in trifluorides  $\text{mf}_3$  ( $m = \text{fe}, \text{cr}, \text{v}$ ),” *Surface science* **469**, 45–54 (2000).
  - 70 Sanghyun Lee, Shuki Torii, Yoshihisa Ishikawa, Masao Yonemura, Taketo Moyoshi, and Takashi Kamiyama, “Weak-ferromagnetism of  $\text{cof}_3$  and  $\text{fef}_3$ ,” *Physica B: Condensed Matter* **551**, 94–97 (2018), the 11th International Conference on Neutron Scattering (ICNS 2017).
  - 71 VE Dmitrienko, EN Ovchinnikova, SP Collins, G Nisbet, G Beutier, YO Kvashnin, VV Mazurenko, AI Lichtenstein, and MI Katsnelson, “Measuring the dzyaloshinskii–moriya interaction in a weak ferromagnet,” *Nature Physics* **10**, 202–206 (2014).
  - 72 R. M. Sattigeri, et al., and C. Autieri, In manuscript (2024).
  - 73 J. Krempaský, L. Šmejkal, S. W. D’Souza, M. Hajlaoui, G. Springholz, K. Uhlířová, F. Alarab, P. C. Constantino, V. Stokov, D. Usanov, W. R. Pudelfko, R. González-Hernández, A. Birk Hellenes, Z. Jansa, H. Reichlová, Z. Šobán, R. D. Gonzalez Betancourt, P. Wadley, J. Sinova, D. Kriegner, J. Minár, J. H. Dil, and T. Jungwirth, “Altermagnetic lifting of kramers spin degeneracy,” (2023), arXiv:2308.10681 [physics.app-ph].
  - 74 K. P. Kluczyk, K. Gas, M. J. Grzybowski, P. Skupiński, M. A. Borysiewicz, T. Fas, J. Suffczyński, J. Z. Domagala, K. Grasza, A. Mycielski, M. Baj, K. H. Ahn, K. Výborný, M. Sawicki, and M. Gryglas-Borysiewicz, “Coexistence of anomalous hall effect and weak net magnetization in collinear antiferromagnet  $\text{mnte}$ ,” (2023), arXiv:2310.09134 [cond-mat.mes-hall].
  - 75 H Dohnomae, K Shintaku, N Nakayama, and T Shinjo, “Structural and magnetic properties of  $\text{cr/sb}$  multilayers,” *Applied surface science* **60**, 807–812 (1992).
  - 76 V.A. Khomchenko, D.A. Kiselev, E.K. Selezneva, J.M. Vieira, A.M.L. Lopes, Y.G. Pogorelov, J.P. Araujo, and A.L. Kholkin, “Weak ferromagnetism in diamagnetically-doped  $\text{bi}_{1-x}\text{axfe}_3$  ( $a = \text{ca}, \text{sr}, \text{pb}, \text{ba}$ ) multiferroics,” *Mate-*

- rials Letters **62**, 1927–1929 (2008).
- <sup>77</sup> G. Beutier, S. P. Collins, O. V. Dimitrova, V. E. Dmitrienko, M. I. Katsnelson, Y. O. Kvashnin, A. I. Lichtenstein, V. V. Mazurenko, A. G. A. Nisbet, E. N. Ovchinnikova, and D. Pincini, “Band filling control of the dzyaloshinskii-moriya interaction in weakly ferromagnetic insulators,” *Phys. Rev. Lett.* **119**, 167201 (2017).
- <sup>78</sup> Igor Mazin, Rafael González-Hernández, and Libor Šmejkal, “Induced monolayer altermagnetism in  $\text{mnp}(\text{s,se})_3$  and fese,” (2023), arXiv:2309.02355 [cond-mat.mes-hall].
- <sup>79</sup> Craig J. Fennie, “Ferroelectrically induced weak ferromagnetism by design,” *Phys. Rev. Lett.* **100**, 167203 (2008).
- <sup>80</sup> Yishu Wang, Yejun Feng, J.-G. Cheng, W. Wu, J. L. Luo, and T. F. Rosenbaum, “Spiral magnetic order and pressure-induced superconductivity in transition metal compounds,” *Nature Communications* **7**, 13037 (2016).
- <sup>81</sup> D. J. Campbell, J. Collini, J. Sławińska, C. Autieri, L. Wang, K. Wang, B. Wilfong, Y. S. Eo, P. Neves, D. Graf, E. E. Rodriguez, N. P. Butch, M. Buongiorno Nardelli, and J. Paglione, “Topologically driven linear magnetoresistance in helimagnetic fep,” *npj Quantum Materials* **6**, 38 (2021).
- <sup>82</sup> Oleksandr V. Pylypovskyi, Sophie F. Weber, Pavlo Makushko, Igor Veremchuk, Nicola A. Spaldin, and Denys Makarov, “Surface-symmetry-driven dzyaloshinskii-moriya interaction and canted ferrimagnetism in collinear magnetoelectric antiferromagnet  $\text{cr}_2\text{o}_3$ ,” (2023), arXiv:2310.13438 [cond-mat.str-el].